Polish J. Chem., **78**, 1165–1181 (2004)

New Methods to Study Thin Organic Films at Electrode Surfaces*

by I. Zawisza[1,2], X. Cai[1], V. Zamlynny[1,3], I. Burgess[1], J. Majewski[4], G. Szymanski[1] and J. Lipkowski[1]

[1]*Department of Chemistry and Biochemistry, University of Guelph, Guelph, Ontario, N1G 2W1 Canada*
[2]*Institute of Physical Chemistry, Polish Academy of Sciences, Warsaw 01-224, Kasprzaka 44/52, Poland*
[3]*Chemistry Department, Acadia University, Wolfville, Nova Scotia, B4P 2R6 Canada*
[4]*MLNSCE, LANSCE-12, Los Alamos National Laboratory, Los Alamos, NM 87545, USA*

(Received May 25th, 2004; revised manuscript June 4th, 2004)

Chronocoulometry, scanning tunneling microscopy (STM), neutron reflectometry (NR) and *in situ* polarization modulation infrared reflection absorption spectroscopy (PM-IRRAS) have been employed to study the properties of a monolayer of *n*-octadecanol at a Au(111) electrode surface. Chronocoulometry has been used to determine the charge density at the electrode surface covered by the film of *n*-octadecanol. The surface pressure of this film was calculated from the charge density data. The film pressure data were used to describe the film properties at the gold solution interface. It has been found that at film pressures larger than 12 mN m^{-1} the monolayer is in a compressed state and at lower film pressures in a decompressed state. STM imaging, NR and PM-IRRAS have been employed to determine the nature of the two states. We have demonstrated that the properties of a monolayer of *n*-octadecanol at the metal-solution interface display many similarities to the properties of an equivalent film at the air-solution interface.

Key words: polarization modulation fourier transform infrared reflection absorption spectroscopy, neutron reflectometry, scanning tunneling microscopy, *n*-octadecanol, Au(111) electrode, differential capacity, chronocoulometry

The face of electrochemistry is changing. Two decades ago electrochemistry was still a traditional science looking rather inward and concerned with measurements of average quantities such as electrode potential, charge or current. These measurements provided phenomenological description of the investigated phenomena. Molecular level interpretation required modeling which does not provide a unique description of an interface and hence interpretations of electrochemical experiments were frequently ambiguous. The last two decades have witnessed the emergence of new spectroscopic, imaging and surface scattering techniques that transformed electrochemistry into a modern and interdisciplinary science. Chemical processes driven by the static electric field at the interface (charge density), potential applied to the electrode (change of Gibbs energy) or by a flow of a constant current (constant flux) can be investigated today at the molecular level with amazing precision and resolu-

* Dedicated to Prof. Dr. Z. Galus on the occasion of his 70th birthday.

tion. However, in the pursuit of novelty, these modern methods are often used without a prior description of the investigated processes at a macroscopic level by traditional electrochemical methods. This approach is a source of new errors often leads to confusion.

The purpose of this paper is to illustrate the power of combining traditional electrochemical techniques with infrared reflection absorption spectroscopy (IRRAS), neutron reflectometry (NR) and scanning tunneling microscopy (STM) techniques to study thin organic films at the electrode surface. The model of our choice is a monolayer of *n*-octadecanol deposited at the gold electrode surface. This system has been extensively investigated in our [1–4] and Bizzotto's laboratories [5–8]. Details of some experiments described in this paper have been published elsewhere [3]. Here we will present new STM data and will combine them with the results of PM-IRRAS and NR studies to show how to achieve a comprehensive description of the field driven transformation of a thin organic film present at an electrode surface. We will an effort to emphasize that a modern description of electrode processes requires a concerted use of both traditional and nontraditional techniques.

EXPERIMENTAL

Octadecanol (Fluka) was recrystallized form ethanol. It was then dissolved in chloroform (Aldrich) to give ~1.0 mg mL^{-1} stock solutions. A few drops of the stock solution, sufficient to give about 3 monolayers of *n*-octadecanol, were injected onto the air-solution interface of an electrochemical cell and left for ~30min to allow the surfactant to spread and the surface pressure to attain the equilibrium spreading pressure, equal to 33 mN m^{-1} [7]. The film was transferred from the air-solution interface to the gold-solution interface using the Langmuir-Schaefer method [9] (also called the horizontal touch) method as shown in Figure 1.

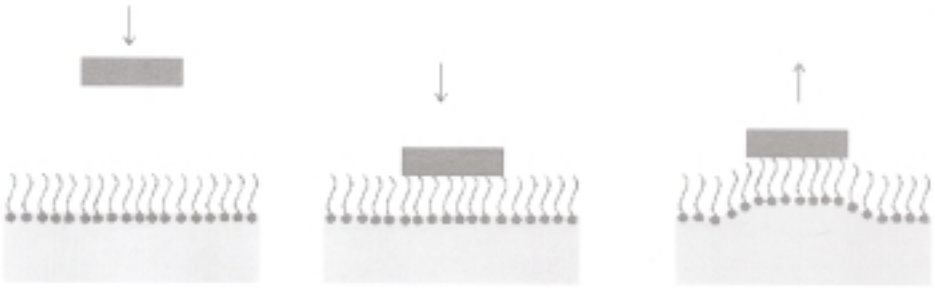

Figure 1. Pictorial description of the horizontal touch method.

The electrochemical measurements were carried out in an all glass three-electrode cell using the hanging meniscus configuration [10]. The Au(111) crystal served as the working electrode (WE) and a Au wire as the counter electrode (CE). The reference electrode was a silver – silver chloride electrode (SSCE) in a saturated KCl solution connected to the cell *via* a salt bridge. A computer-controlled system, consisting of a HEKA potentiostat/galvanostat, a HEKA scan generator (Lambrecht/Pfalz, Germany) and a lock-in amplifier, EG&G Instruments 7265 DSP (Cypress, CA), was employed to perform electrochemi-

cal experiments. All electrochemical data were acquired *via* a plug-in acquisition board (National Instruments PCI 6052E) and custom-written software generously provided by Professor Dan Bizzotto of the University of British Columbia. The differential capacity curves were determined using a scan rate of 5 mV s^{-1} and an ac perturbation with 25 Hz frequency and 5 mV r.m.s. amplitude. The differential capacity curves were calculated from the in-phase and the out-of-phase components of the ac signal assuming a simple series RC equivalent circuit.

The charge density at the electrode surface was determined using the chronocoulometric method [11]. The gold electrode was held at a base potential E_b = 0.0 V for 30 s. Then the potential was stepped to a variable potential of interest E_f, where the electrode was held for a time, t_f, equal to 20 s. Next, a potential step to the desorption potential E_{des} = –0.725 V was applied for 150 ms and the current transient corresponding to the desorption of the film and recharging of the interface was recorded. Finally, the potential was stepped back to E_b for 30 s before new potential steps to E_f and from E_f to E_{des} were applied. The integration of the current transients gives the difference between charge densities at potentials E_f and E_{des}. Similar experiments were performed at the film free electrode in the pure supporting electrolyte. The absolute charge densities were then calculated using the independently determined potential of zero charge (pzc) E_{pzc} = 0.31 V *versus* (SSCE). Prior to experiments the electrode was cleaned by flame annealing. Electrochemical experiments were carried out in 0.1 M NaF supporting electrolyte. IR measurements were performed in 0.1 M NaF dissolved in D_2O (Cambridge Isotopes LTD).

STM images were acquired using the procedure described in [12] with the help of the Nanoscope E (Digital Instruments, Santa Barbara, CA) instrument equipped with the A scanner. STM-tips were electrochemically etched tungsten wires coated with polyethylene. All STM images were recorded in constant current mode with tunneling currents ranging between 0.2 and 20 nA. The working electrode used in STM experiments was a small bead produced by melting an end of a gold wire that was spot welded to a gold plate. The working electrode was cleaned by flame annealing before each experiment.

The details of the PM IRRAS experiments were described in our previous publications [3,13]. The Nicolet, Nexus 870 (Madison, WI) spectrometer, equipped with an external TOM table, MCT-A detector, photoelastic modulator (Hinds Instruments PM-90 with II/ZS50 ZnSe 50 kHz optical head, Hillsboro, OR) and demodulator (GWC Instruments Synchronous Sampling demodulator, Madison, WI) was used to perform PM -IRRAS experiments. The spectra were acquired using in house software, an Omnic macro and digital-to-analog converter (Omega, Stamford, CT) to control the potentiostat (HEKA PG285, Lambrecht/Pfalz, Germany) and to collect spectra. The IR window was a 1 inch equilateral BaF_2 prism (Janos Technology, Townshead, VT). Prior to the experiment, the window was washed in water and methanol and then cleaned for 20 minutes in an ozone chamber (UVO-cleaner, Jelight, Irvine, CA).

Figure 2 shows the diagram of the spectroelectrochemical cell used in these experiments. Prior to the assembly of the spectroelectrochemical cell, a monolayer of *n*-octadecanol was transferred onto the Au(111) surface by the horizontal touch method. After the organic film was deposited onto the electrode surface, the cell was filled with the electrolyte and argon was purged through the solution to remove oxygen. The electrode was then pressed against the BaF_2 window to form a thin layer configuration. A starting potential of E = 0.20 V(SSCE) was applied to the electrode and spectra were collected in a series of potential steps. Initially, the potential was stepped in the negative direction using a step increment of either 0.050 or 0.2 V until a negative potential limit (potential at which the film is detached from the electrode surface) was reached. At this point the direction of potential steps was reversed and spectra were collected at either 0.050 or 0.2 V intervals up to E = 0.20 V (SSCE). For this initial cycle of steps, 1000 scans were recorded at every potential. Subsequently, the cyclic series of potential steps was repeated 20 times so that a total of 8000 scans were recorded at each potential. The instrument resolution was 2 cm^{-1}. At the end of the measurement the scans were individually checked for anomalies using an automated software macro and then averaged for each potential.

The IR signal was corrected for the PEM response functions and background. When all these corrections are carried out, the background corrected spectrum plots ΔS, which is proportional to the absorbance A of the adsorbed molecules as shown by equation 1:

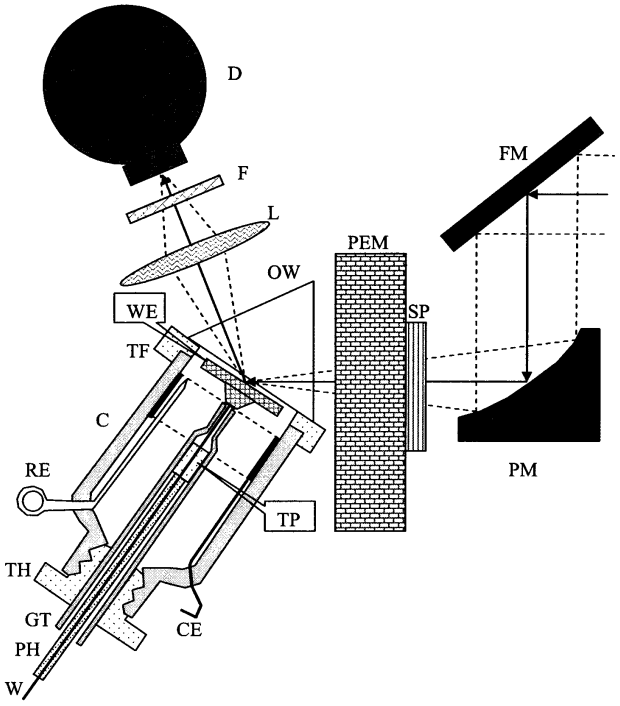

Figure 2. Diagram of the spectroelectrochemical cell used in the PM-IRRAS experiments; The beam path indicated by a solid line with arrows; FM – flat mirror, PM – parabolic mirror, SP – static polarizer, PEM – photoeleastic modulator, OW – optical window (BaF_2 prism bellowed at 60°), L – ZnSe focusing lens, F – filter, WE – working electrode, RE – reference electrode, CE – counter electrode, TP – teflon plug, TH – teflon holder, GT – glass tube, PH – piston handle.

$$\Delta S = \frac{2(I_s - I_p)}{I_s + I_p} = 2.3A = 2.3\Gamma\varepsilon \tag{1}$$

where ε is the decimal molar absorption coefficient and Γ is the surface concentration of the adsorbed species [3,13].

Neutron reflectivity experiments were carried out on the NG-7 reflectometer at the National Institute of Standards and Technology (NIST) in Gaithersburg, Maryland. The working electrode was derived from a polished single – crystal (~82 mm × ~38 mm × ~13 mm) quartz substrate obtained from CrysTec GmbH (Berlin, Germany). Thin layers of chromium and gold were sequentially sputtered on the substrates. The resistance of the thin film of gold was on the order of a few ohms. Figure 3 shows a diagram of the electrochemical cell designed for these measurements. This is a modified version of the cell used in previous experiments [14]. An "inverted" geometry, in which the gold-coated quartz electrode was above the solvent phase, was used in our experiments.

A film of *n*-octadecanol was spread at the surface of water in a small Langmuir trough at the equilibrium spreading pressure and transferred onto the dry, gold-coated surface of the quartz crystal using a single touch, Langmuir-Schaefer technique. The electrolyte solution was 50 mM $KClO_4$ prepared in D_2O (99.9%, Sigma). The electrolyte solution was degassed with argon and then introduced into the inlet of the Teflon cell. The reference electrode was then placed in an arm leading into the Teflon block.

Neutron reflectivity measures the normalized (by the incident flux) intensity of specularly reflected neutrons as a function of the momentum transfer vector Q_z:

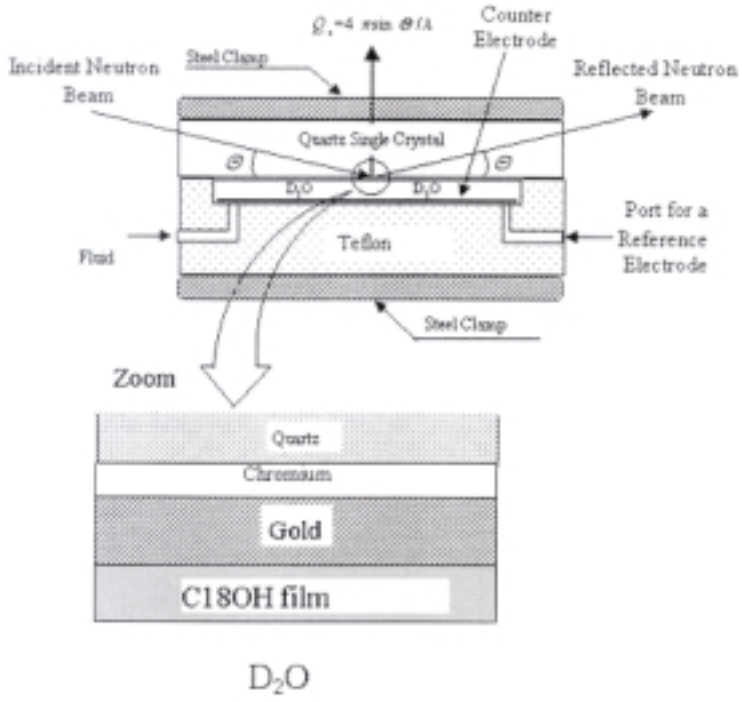

Figure 3. Diagram of the electrochemical cell used for neutron reflectometry studies at the gold-solution interface.

$$Q_z = \frac{4\pi \sin\theta}{\lambda} \tag{2}$$

where θ is the angle of the incidence and λ is the neutron de Broglie wavelength. A fixed neutron wavelength of 4.75 Å was used and Q_z was varied by changing the angle of incidence. The error points on the data represent the statistical errors in the measurements (standard deviation σ). A constant instrumental resolution of $\Delta Q_z/Q_z = 0.043$ (FWHM) was used throughout the scan. Varying the angle of incidence allowed reflectivities to be measured in the Q_z range of ~ 0.0 to up to 0.15 $Å^{-1}$. The data were reduced taking into account the neutron beam transmission through the quartz substrate and corrected for the background. The scattering length density (SLD) and the film thickness data were determined by fitting a model to the reflectivity curve using the Parratt 32 fitting algorithm [15].

RESULTS AND DISCUSSION

Chronocoulometry has been applied to describe the transfer of a film of *n*-octadecanol from the gas-solution onto the metal solution interface quantitatively. A monolayer of *n*-octadecanol was spread at the gas-solution interface of the electrochemical cell and the gold electrode was horizontally approached at a controlled potential 0.2 V (SSCE) until contact with the gas-solution interface was made. The chronocoulometric experiments were then performed to determine the charge density at the electrode surface. Figure 4A plots the charge density *versus* potential for the

electrode covered by the film and in the absence of the film. Three series of measurements were performed. In series one, for each potential the film was freshly transferred onto the electrode surface and only one potential step to E_{des} was applied. To acquire the next point on this plot, the electrode was withdrawn, flame annealed and horizontally touched to the air-solution interface. In series two, the film was transferred to the gold-solution interface once and then exposed to multiple adsorption-desorption cycles by applying a train of potential pulses with the value of E_f progressively increasing from –0.75 V (SSCE) to 0.4 V (SSCE) (positive train of pulses). In series three, the film was transferred only once and then periodically desorbed and re-adsorbed using a negative train of pulses with E_f progressively decreasing from 0.4 V (SSCE) to –0.75 V (SSCE).

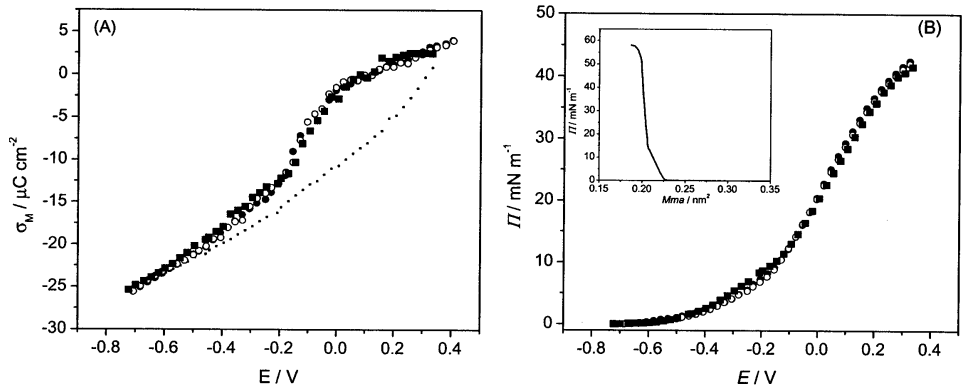

Figure 4. A) Charge density *versus* potential plots and B) surface pressure *versus* potential plots for various sequences of the potential pulses; (filled squares) – first desorption, each point corresponds to the freshly deposited film that was not desorbed at $E = –0.8$ V; (filled circles) film formed once and being repeatedly adsorbed and desorbed using train of potential pulses progressively decreasing amplitude (negative potential steps), (open circles) film formed once and being repeatedly adsorbed and desorbed using train of potential pulses with progressively increasing amplitude (positive potential steps), (small squares) charge on the film free Au(111) electrode in 0.1 M NaF supporting electrolyte. Inset: The Langmuir isotherm of *n*-octadecanol recorded on the air – 0.1 M NaF solution interface.

Quite similar charge density plots were obtained for each of these three series of measurements. The data indicate that the film is desorbed from the electrode surface at $E < –0.6$ V (SSCE) and is adsorbed at more positive potentials. The charge density curves display two steps. The first small step may be seen for $–0.5 \text{ V} < E < –0.1$ V (SSCE). The second big step is located at $–0.1 \text{ V} < E < 0.4$ V (SSCE). Such behaviour indicates that adsorption of *n*-octadecanol at the Au(111) electrode surface has a two state character.

The area between the charge density curves for the film free and the film covered electrode is equal to the change of the interfacial energy at the gold-solution interface

caused by adsorption of the film. The energy per unit surface area is equal to the film pressure. Figure 4B plots the film pressure calculated by integration of the charge density curves *versus* the electrode potential. The film pressure curve attains a maximum value of ~43 mN m^{-1} at ~0.4 V (SSCE). This curve consists of two overlapping bell shape curves that intersect at π ~12 mN m^{-1}. The inset in Figure 4B plots an isotherm determined for the compression of a monolayer of *n*-octadecanol at the air-solution interface of a Langmuir trough. The compression isotherm shows two linear segments with a different slope (different compressibility), indicating that the monolayer of *n*-octadecanol display a two state behaviour at the air-solution interface as well. The phase transition (the discontinuous point in the isotherm) is observed at π ~12 mN which is the same value of the film pressure at which a phase transition is observed at the gold solution interface.

To summarize this section, electrochemical (chronocoulometric) measurements shown that the monolayer of *n*-octadecanol may be transferred from the gas-solution interface onto the gold solution interface. The monolayer is adsorbed at the gold surface at small charge densities and is desorbed when charge densities become large. The monolayer of *n*-octadecanol adsorbed at the gold surface has comparable film pressure to the monolayer spread at the air-solution interface. When the electrode potential is moved from 0.4 V (SSCE) in negative direction, the film pressure decreases and at $E \sim -0.1$ V (SSCE) a phase transition is observed at π ~12 mN. Similar behaviour is observed at the air-solution interface when a monolayer of *n*-octadecanol is decompressed by changing the position of the movable barrier at the surface of a Langmuir trough. This result suggests that by applying potential to the gold electrode one can compress or decompress the film in a similar manner as by moving the barrier at the surface of a Langmuir trough.

X-ray diffraction studies performed on a monolayer of *n*-octadecanol at the air-solution interface demonstrated that at room temperature this film behaves as a two dimensional solid [18]. To determine the structure of the film at the gold-solution interface, we have performed STM studies. Figure 5 shows an image of a 30×30 nm section of the Au(111) surface covered by the monolayer of *n*-octadecanol. The experiments were performed in the electrochemical cell of the Nanoscope E at a controlled electrode potential. The image shows rows of well ordered molecules that appear to assume a vertical or tilted orientation. The white spots on the image correspond to gold islands of monoatomic height, dispersed on the otherwise atomically flat 30×30 nm section of the surface.

The upper right corner of the image shows a defected section of the film in which the molecules appear to assume a flat orientation. In fact, such defected film regions were much larger in other areas of the electrode surface. Figure 6 shows a high resolution image of the film of *n*-octadecanol at the gold electrode surface by zooming into the defected section of the film. The quality of the image is very high and one can easily see individual *n*-octadecanol molecules lying flat at the gold surface and assembled into a periodic stripe like pattern. The width of a stripe is equal to ~4.9 nm and this is approximately equal to the length of two fully stretched *n*-octadecanol mole-

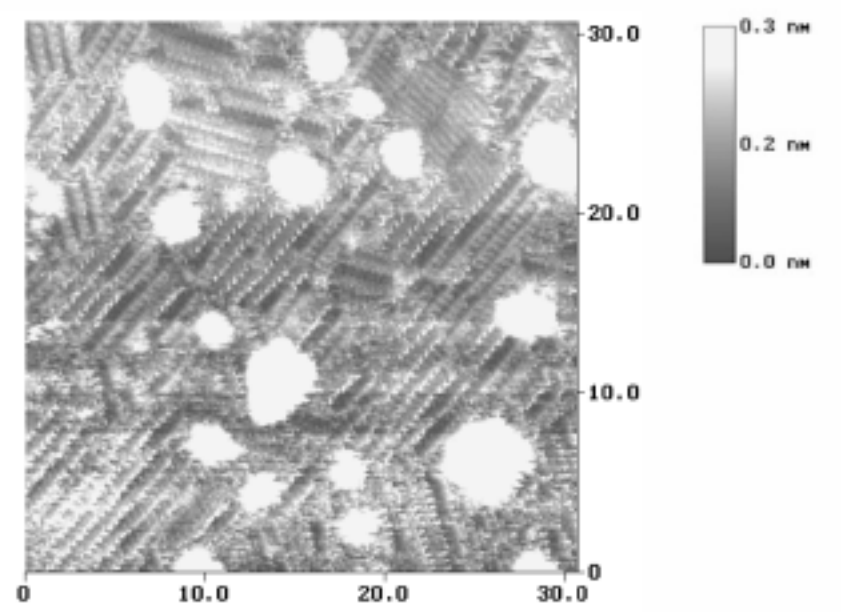

Figure 5. STM image of a Au(111) electrode surface covered by a monolayer of *n*-octadecanol at E = 250 mV (SSCE). Tip bias potential 150 mV, tip current 300 pA, scan rate 10 Hz.

cules [19]. One can even distinguish the head and tail regions of the individual molecule. Furthermore, one can see that each periodic stripe consists of two rows of *n*-octadecanol molecules. The molecules in one row (one layer) are turned with their tails directed toward the tails of the molecules in the second row (second layer) such that the stripe looks like a cross section of a biological bilayer. In this arrangement, the hydrophobic (non-polar) region of one molecule is in contact with the hydrophobic region of another molecule and the polar head is in contact with another polar head.

The defected domains may actually be quite large. Figure 7 shows a 60×60 nm section of the surface covered by a defected film. One can easily see that the stripes of flat lying molecules are very long. At this magnification, one also can see additional chevron-like lines that run almost perpendicular to the stripes of the flat lying *n*-octadecanol molecules. These are the characteristic lines of the (1×23) reconstruction of the Au(111) surface. Flame annealing is known to cause the Au(111) surface to reconstruct [20,21]. It is also known that the reconstructed surface is favoured when the gold surface is negatively charged and that the reconstruction is lifted when the surface is positively charged [22]. Our earlier surface X-ray scattering studies demonstrated that adsorption of organic molecules may stabilize the reconstructed surface [23]. The present STM data show that the film of *n*-octadecanol is transferred onto a reconstructed Au(111) surface and that adsorbed *n*-octadecanol molecules stabilize this structure.

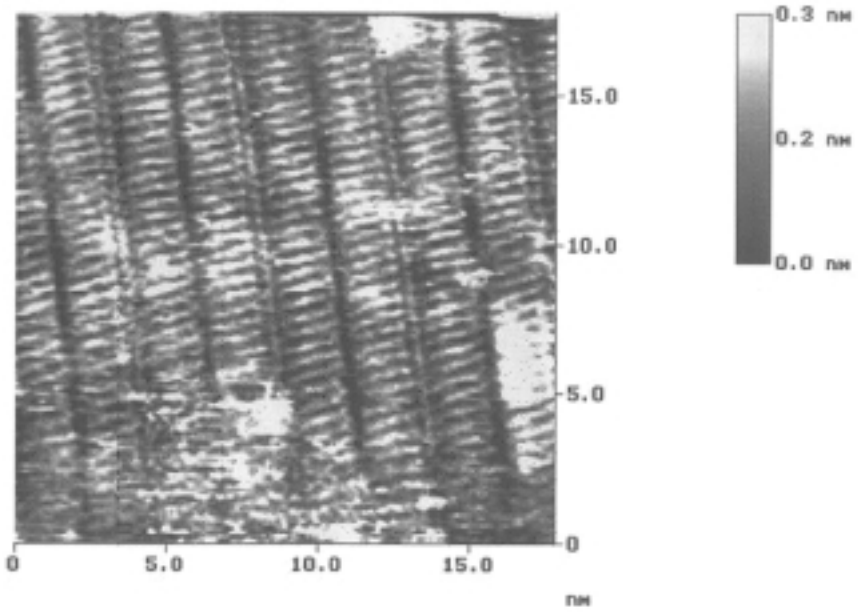

Figure 6. High resolution STM image of a defected area of the film showing flat lying individual *n*-octadecanol molecules at E = 250 mV (SSCE). Tip bias potential 150 mV, tip current 300 pA, scan rate 10 Hz.

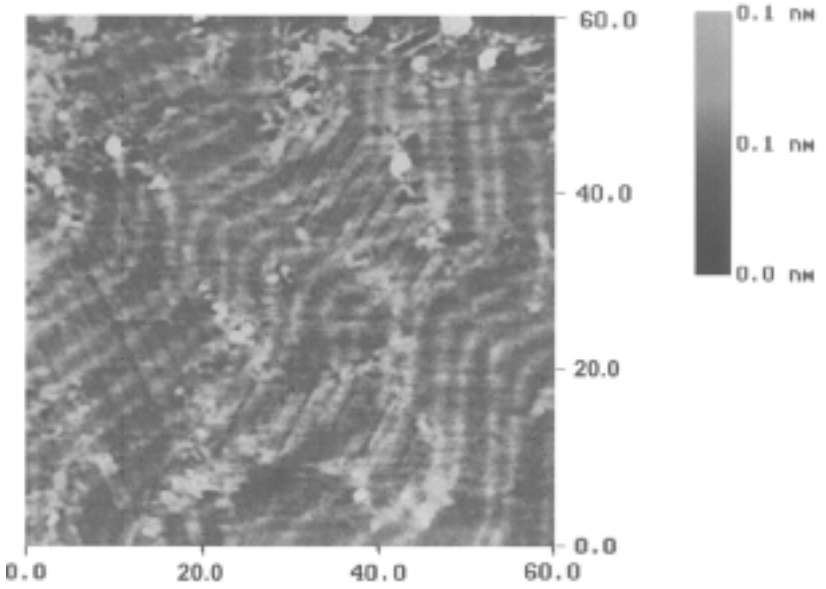

Figure 7. Lower resolution STM image of the Au(111) surface covered by a film of flat lying *n*-octadecanol molecules at E = 250 mV (SSCE). The presence of a characteristic chevron pattern indicates that the Au(111) is reconstructed and that adsorption of *n*-octadecanol molecules does not lifts the reconstruction. Tip bias potential 150 mV, tip current 300 pA, scan rate 10 Hz.

STM measurements provided important structural information that complements the knowledge gained from chronocoulometric studies. They demonstrated that the monolayer of *n*-octadecanol adsorbs at the reconstructed Au(111) surface and that it stabilizes rather than lifts the reconstruction. They also showed that the film of *n*-octadecanol molecules has a two dimensional solid like structure. Further, these measurements demonstrated that some sections of the Au(111) surface are covered by vertically oriented *n*-octadecanol molecules while other sections by flat lying molecules. We refer to the domains of flat lying molecules as defected domains. However, STM probes only a small fraction of the electrode surface and with this technique it is difficult to determine whether the film consists predominantly of vertically or flat lying molecules.

Neutron reflectometry has therefore been employed to determine the predominant structure of the film of *n*-octadecanol at the Au(111) electrode surface. Figure 8 contains the basic information needed for the interpretation of the NR data. Neutrons are reflected from an interface when the two neighbouring phases have different refractive indexes. The equation in the top left panel of Figure 8 shows that the refractive index of a given phase is related to the scattering length density (SLD) ρ. The SLD is determined by the combined nuclear spin state of the nucleus-neutron scattering system and consequently depends on the nuclear composition of the film. It is proportional to the number density of a given isotope. The table in Figure 8 lists numerical values of the scattering length density for various materials employed in our experiments. One can note that a particularly large contrast of the scattering length density and therefore good reflectivity is achieved when a film of hydrocarbon molecules is deposited onto a gold electrode surface and D_2O is used as the aqueous phase.

The bottom left panel of Figure 8 shows typical reflectivity curves recorded for the reflection of neutrons at the gold/D_2O interface with and without a film of hydrocarbon (h-C18OH) molecules. At small angles of incidence (Q_z less than the critical value Q_c) the beam is totally reflected and the reflectivity is equal to unity. When Q_z becomes larger than Q_c the reflectivity decreases quickly and its change with Q_z is described by the following formula [24]:

$$R(Q_z) = \frac{(4\pi)^2}{Q_z^4} f(\rho) \tag{3}$$

in which the first term describes the Fresnel reflectivity from a single interface (two phase system) and the second term is a function of the SLD (ρ) profile in the direction normal to the surface. In the absence of the film the reflectivity decreases monotonously with Q_z proportionally to Q_z^{-4}. In the presence of the film the reflectivity curve displays characteristic oscillations due to the constructive and destructive interference between beams reflected from the gold-organic layer and the organic layer-D_2O interfaces. The periodicity of these oscillations depends on the thickness of the film and the amplitude depends on the SLD profile in the direction normal to the interface.

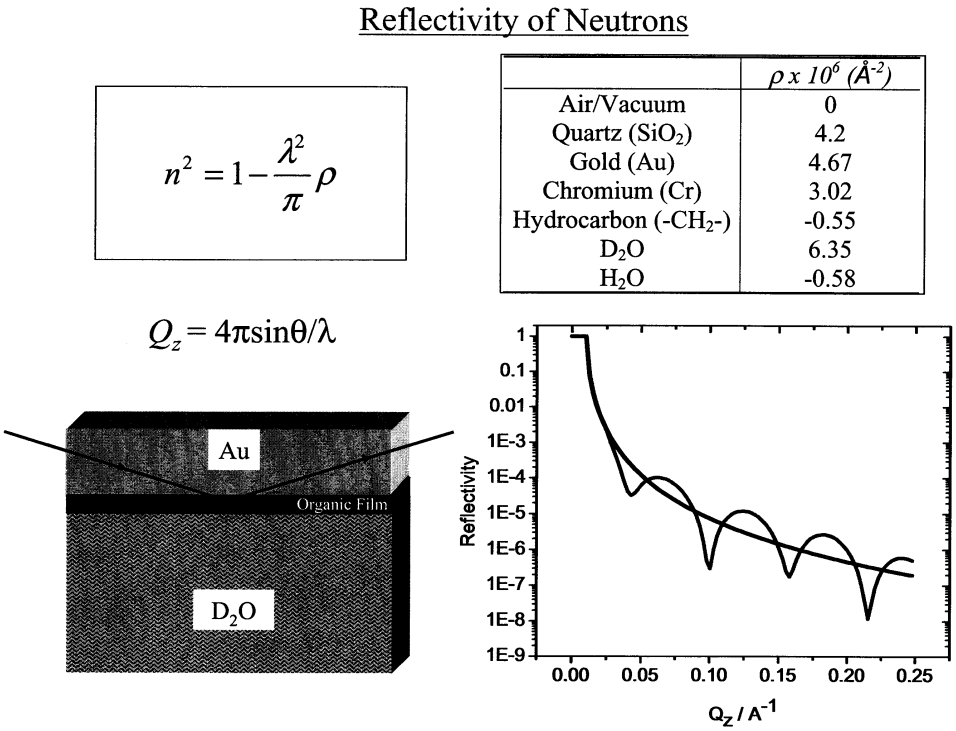

	ρ x 10^6 (Å^{-2})
Air/Vacuum	0
Quartz (SiO_2)	4.2
Gold (Au)	4.67
Chromium (Cr)	3.02
Hydrocarbon (-CH_2-)	-0.55
D_2O	6.35
H_2O	-0.58

Figure 8. Principles of the neutron reflectometry at the solid-liquid interface.

Thus the neutron reflectivity can provide valuable information concerning the average thickness of the film and its composition (D_2O content in the film).

The top panel in Figure 9 plots the reflectivity *versus* the momentum transfer vector curve for the film of hydrogenated $C_{18}OH$ deposited on a block of quartz covered with a ~3 nm layer of Cr and ~8 nm thick layer of gold. The panel shows two curves recorded for potentials of the two adsorption states identified earlier with the help of chronocoulometric experiments. The curve at 100 mV (SSCE) corresponds to the film pressure above 12 mN m^{-1} (compressed state) and the curve at –300 mV to the film pressure less than 12 mN m^{-1} (decompressed state). The points with error bars plot the experimental data, the solid lines are the best fits to the data that give the SLD profiles in the direction normal to the interface shown in bottom panel of Figure 9.

The SLD profiles allow one to estimate the thickness and D_2O content in the film. For the film at 100 mV the film thickness is ~2.2 nm, however the volume fraction of D_2O in the film is ~40%. For the film at –300 mV the thickness of the film decreases to ~2.1 nm however the D_2O content in the film increases to 60%. The neutron reflectivity data are consistent with the results of the STM experiments. They indicate that at potentials close to the pzc the vertical orientation of *n*-octadecanol molecules in the film predominates. However, large sections of the film are defected and the defects are filled with water. They also show that the film thickness decreases when the film is decompressed and concomitantly the water content in the film increases. The change

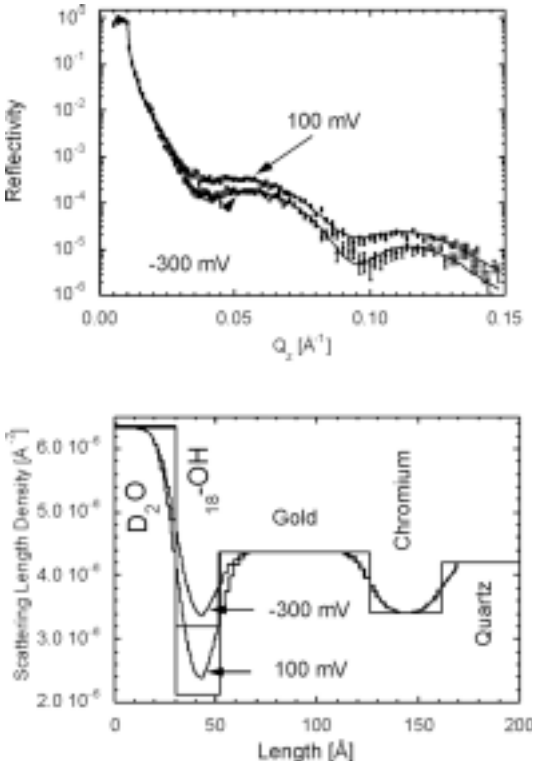

Figure 9. Top panel reflectivity *versus* the momentum transfer plots determined for the *n*-octadecanol film at the gold solution interface for two selected potentials. Bottom panel, scattering length density in the direction normal to the interface determined from the neutron reflectivity plots.

of the film thickness suggests that the tilt angle of *n*-octadecanol molecules in the film changes with the electrode potential. The thickness of a monolayer of fully stretched vertically oriented *n*-octadecanol molecules is equal to 2.4 nm [19]. Using this number, one can calculate that *n*-octadecanol molecules are tilted at 8° with respect to the normal in the film at 100 mV and at 18° at $E = -300$ mV.

The tilt angle may be independently measured using IR reflection spectroscopy. Figure 10 pictorially illustrates the surface selection rules for the reflection of IR photons from a gold surface. When a linearly polarized beam of IR radiation is incident on the metal, the strength of the electric field of the photon at the surface depends on the photon polarization. For *p*-polarized photons (where the electric field of the photon is located in the plane of incidence defined by the location of the incident and reflected beams), the incident and reflected beams interact constructively and the field strength of the photon is enhanced. For the *s*-polarized photon (where the direction of the electric field of the photon is perpendicular to the plane of incidence and is parallel to the surface), the reflected beam is 180° phase shifted with respect to the incident beam and at the point of reflection (*i.e.* the metal surface) the interference between the two beams is destructive. The electric field of the *s*-polarized photon at the metal surface is close to zero [25].

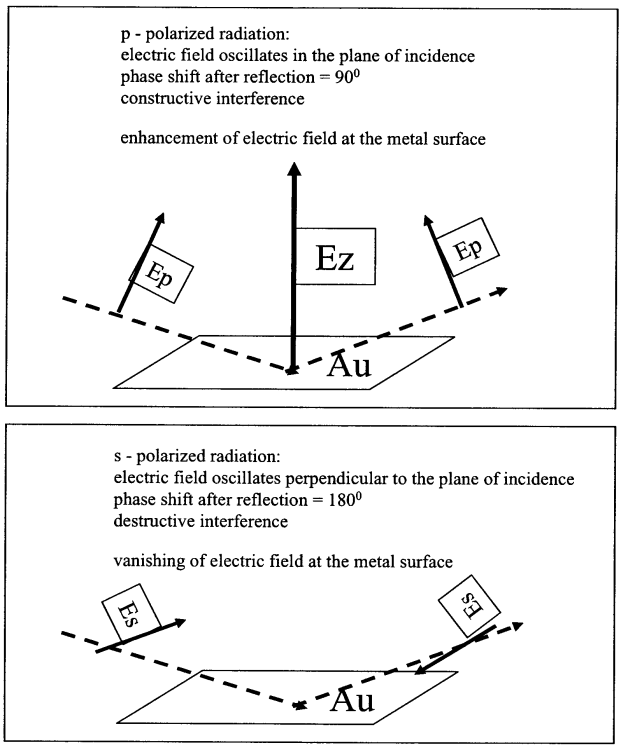

Figure 10. Surface selection rules for reflection of a linearly polarized IR beam at the gold electrode surface. Top panel *p*-polarized beam, bottom panel *s*-polarized beam.

We have employed PM IRRAS spectroscopy to measure the IR spectra of *n*-octadecanol molecules at the gold electrode surface. In this technique the polarization of the incident photon is periodically changed between *p*- and *s*-. When a *p*-polarized photon is incident upon the gold surface it is absorbed by the film. In contrast, the *s*-polarized photon has zero field strength at the surface and is not absorbed by the film. The difference between the intensities of the *p*- and *s*-polarized beams is measured and divided by the average beam intensity. In that way, the absorbance of all elements present in the optical path except the film is cancelled and the measured signal plots the spectrum of the film of adsorbed molecules.

Figure 11 plots the PM-IRRAS spectra in the CH stretching region of the *n*-octadecanol monolayer. Spectra marked "first desorption" were acquired for a freshly deposited film by changing the potential from 0.2 V (SSCE) in the negative direction (desorption scan). Spectra marked "re-adsorption" were recorded when the potential is again changed from 0.2 V (SSCE) in the negative direction (re-desorption scan) following re-adsorption of the previously desorbed film. Three strong CH stretch bands at 2958 cm^{-1}, ~2915 cm^{-1} and 2850 cm^{-1} correspond to $\nu_{as}(CH_3)$, $\nu_{as}(CH_2)$ and $\nu_s(CH_2)$, respectively. The position of the CH_2 stretch bands is sensitive to conformational changes of the alkyl chains [26–28]. The frequencies of $\nu_{as}(CH_2)$ less than 2920 cm^{-1} and $\nu_s(CH_2)$ less than 2851 cm^{-1} indicate that monolayers of

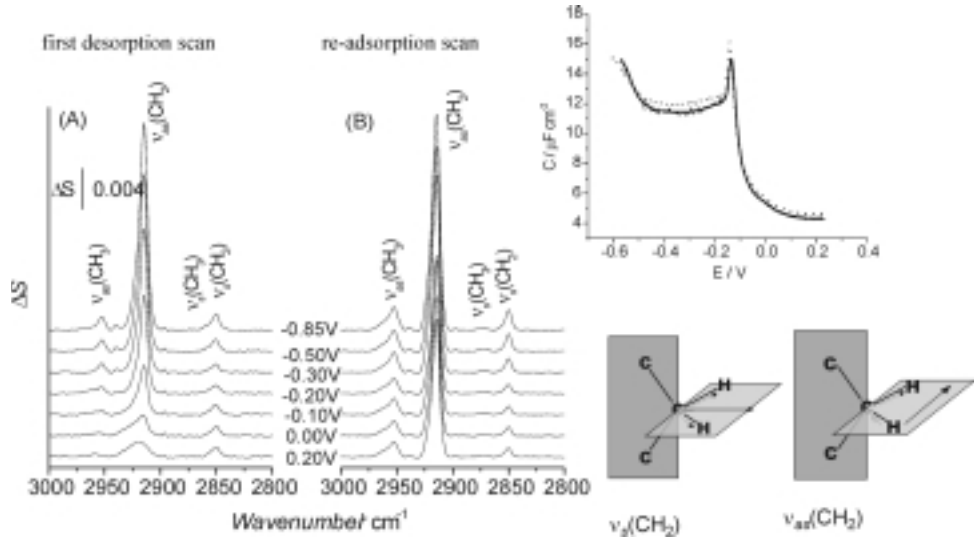

Figure 11. PM-IRRAS spectra recorded for a monolayer at the Au(111) electrode recorded in the first desorption and the readsorption scans. Upper right corner, differential capacity curves recorded in the first desorption (solid line) and the second desorption (dotted line) scans. Cartoons in the bottom right corner show directions of transition dipoles of the symmetric and asymmetric CH_2 stretches.

n-octandecanol are in the 2D solid state and that the hydrocarbon chains are fully stretched in an *all trans* zigzag orientation [26].

For the freshly formed film, the intensity of the $\nu_{as}(CH_2)$ band changes significantly with potential. The changes with potential are much smaller in the re-adsorbed film. The intensities of the $\nu_s(CH_2)$ band also display much smaller dependence on the electrode potential. This behaviour points to pronounced changes in the orientation and/or rotation of *n*-octadecanol molecules in the freshly formed and the re-adsorbed films. The graph in the upper right corner of Figure 11 shows the differential capacity curves of the Au(111) electrode recorded during the first desorption and the re-adsorption scans. In contrast to pronounced differences between the IR band intensities recorded in these two scans, the differences between the two capacity curves are very small. This is a good example of the ability of *in situ* IR spectroscopy to reveal orientational changes in the film of organic molecules that are barely visible when only classical electrochemical measurements are employed.

The cartoons in the lower right corner of Figure 11 show the directions of the transition dipoles of the $\nu_{as}(CH_2)$ and $\nu_s(CH_2)$ bands. The angle between the direction of the transition dipole moment and the direction normal to the surface (direction of the

electric field vector of the photon) (θ) can be calculated from the integrated intensities of the IR bands using the following equation [29]:

$$\cos\theta = \frac{1}{3}\,\frac{A_{(E)}}{3A_{(random)}} \tag{4}$$

where: $A_{(E)}$ is the integrated intensity of the IR band at a given potential and $A_{(random)}$ is the integrated intensity of the band for a random distribution of molecules in the film. The directions of the transition dipole moments of the asymmetric and the symmetric CH_2 stretches are orthogonal to each other and form a 90° angle with the line of a fully extended all trans hydrocarbon chain. Therefore, the angles θ_{as} and θ_s and the tilt angle of the chain θ_{chain} are related by the formula [30]:

$$\cos^2\theta_{as} + \cos^2\theta_s + \cos^2\theta_{\text{chain}} = 1 \tag{5}$$

from which the tilt angle of the chain can be calculated.

Figure 12 plots θ_{chain} as a function of the electrode potential. Details of the θ_{chain} calculations and the determination of $A_{(random)}$ are described in [3]. Full squares mark the first desorption scan (voltage scanned in negative direction) and the full circles mark the first re-adsorption scan (voltage scanned in the positive direction). At E = 100 mV, for a freshly deposited monolayer the hydrocarbon chains assume a small tilt angle of ~12°. This number is close to the tilt of 8° determined from neutron reflectivity data. By moving E in the negative direction, the tilt angle increases. At E = –300 mV, the tilt angle is 23°. A somewhat smaller angle of 18° was determined from the neutron reflectivity experiments. In the re-adsorbed film a much higher tilt angle ~22°

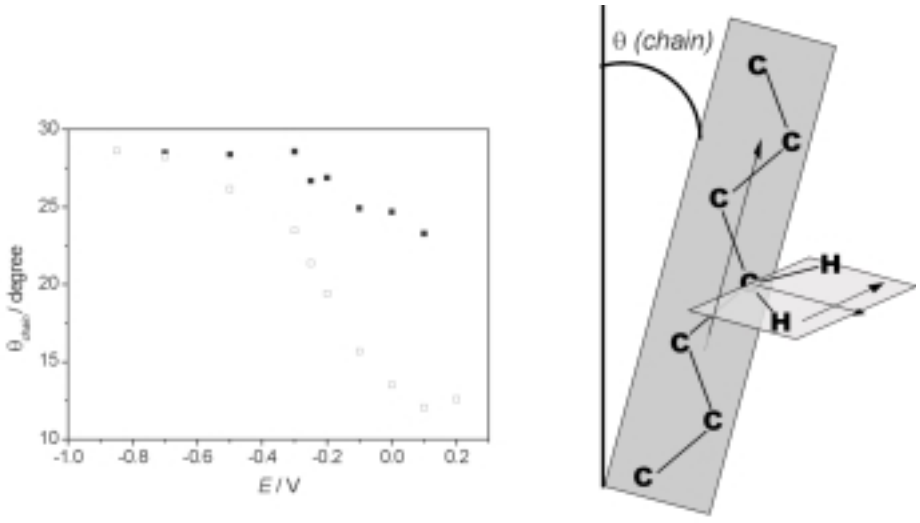

Figure 12. Change of the chain tilt angle with the electrode potential; (open squares) – first desorption scan, (black squares) – re-adsorbed film. Cartoon shows the definition of the tilt angle.

is observed at E = 100mV. This behaviour suggests that the freshly formed film is more ordered than the re-adsorbed film.

Figure 12 shows that the tilt angle changes little with potential for $E > -100$ mV (or when the film pressure is higher than 12 mN m^{-1}) and increases steeply with E at more negative potentials (when film pressure is less 12 mN m^{-1}). Apparently, the monolayer of *n*-octadecanol displays similar behaviour at the metal-solution and the air solution interfaces. Depending on the value of the film pressure, the monolayer may exist in the compressed or decompressed states. The potential applied to the electrode controls the film pressure at the metal-solution interface while it is the movable barrier in a Langmuir trough that controls the film pressure at the air-solution interface. In the first case, the electrical energy and in the second case the mechanical energy is used to change the pressure of the film. Our results show that the structure of the octadecanol film does not depend on the external stimulus used to compress the film.

CONCLUSIONS

We have applied "traditional" (electrochemical) and "non-traditional", STM, neutron reflectivity and PM-IRRAS techniques to study the properties of a monolayer of *n*-octadecanol transferred from the gas-solution onto the metal-solution interface of a gold electrode. The "traditional" electrochemical measurements have provided a phenomenological description of the properties of this film at the electrode surface. We learnt that the film is adsorbed at the gold surface at $E > -0.6$ V and that it is desorbed at more negative potentials. We were also able to determine the film pressure for the monolayer at the electrode surface. We observed that the film undergoes a phase transition at potential where π = ~12 mN m^{-1}. A monolayer of *n*-octadecanol molecules at the air-water interface undergoes a phase transition from a compressed to a decompressed state at exactly the same film pressure.

The use of "nontraditional" techniques provided insight into the film structure at the molecular level. The STM images demonstrated that the film is well ordered. They have also shown that the film consist of domains in which *n*-octadecanol molecules are oriented vertically and domains in which the molecules are lying flat on the surface. The neutron reflectivity measurements confirmed that the film has a patchy structure with sections covered by vertically oriented molecules and defected sections that contain water. However, these measurements showed that the film thickness is comparable in magnitude to the length of a fully stretched *n*-octadecanol molecule. They therefore demonstrated that the vertical orientation of the molecules is the predominant orientation and that the STM images of flat lying molecules represent defected sections of the film. The NR data also showed that the thickness of the film changes with the electrode potential.

The conclusions reached based on the NR studies were confirmed by independent *in situ* IR reflection spectroscopy experiments. With the help of the PM-IRRAS technique we learned that chains of adsorbed *n*-octadecanol molecules are fully stretched

out into the *all-trans* conformation. Using IR data, we were able to study how the tilt angle of the chains changes with the electrode potential. These results helped us to understand why a monolayer of *n*-octadecanol has similar properties at the metal-solution and at the air-solution interfaces. The state of the film is controlled by the film pressure, which at the metal-solution interface is controlled by potential and at the air-solution interface of a Langmuir trough by the movable barrier. We have demonstrated a need for concerted use of "traditional" and "nontraditional" methods to study the properties of thin organic films at electrode surfaces.

Acknowledgments

This work has been supported by a grant from the Natural Sciences and Engineering Council of Canada (NSERC). JL acknowledges the Canada Research Chair Award of the Canada Foundation for Innovation.

REFERENCES

1. Bizzotto D., Noel J.J. and Lipkowski J., *J. Electroanal. Chem.*, **369**, 259 (1994).
2. Bizzotto D. and Lipkowski J., *Progress Surf. Sci.,* **50**, 237 (1995).
3. Zawisza I., Burgess G., Szymanski G., Lipkowski J., Majewski J. and Satija S., *Electrochim. Acta,* in press.
4. Zawisza I. and Lipkowski J., *Langmuir,* **20**, 4579 (2004).
5. Yang Y. and Bizzotto D., *J. Electroanal. Chem.,* **500**, 408 (2001).
6. Shephard J.L. and Bizzotto D., *J. Phys. Chem. B*, **117,** 8524 (2003).
7. Bizzotto D., Wong E. and Yang Y., *J. Electroanal. Chem.,* **480**, 233 (2000).
8. Bizzotto D. and Pattinger B., *Langmuir*, **15***,* 8309 (1999).
9. Langmuir I. and Schaefer V.J., *J. Am. Chem. Soc.,* **60**, 1351 (1938).
10. Dickertmann D., Schultze J.W. and Koppitz F.D., *Electrochim. Acta*, **21**, 967 (1976).
11. Richer J. and Lipkowski J., *J. Electrochem. Soc.,* **133**, 121 (1986).
12. Burgess I., Jeffrey C.A., Szymanski G., Galus Z. and Lipkowski J., *Langmuir,* **15**, 2607 (1999).
13. Zamlynny V., Zawisza I. and Lipkowski J., *Langmuir,* **19**, 132 (2003).
14. Burgess I., Zamlynny V., Szymanski G., Schwan A.L., Faragher R.J., Lipkowski J., Majewski J. and Satija S., *J. Electroanal. Chem.*, **187**, 550 (2003).
15. Braun C., The Reflectivity Tool. *Parratt 3.,* (1999) HMI, Berlin.
16. Kaganer V.M., Mohwald H. and Dutta P., *Rev. Modern Phys.*, **71**, 779 (1999).
17. Durbin M.K., Shih M.C., Malik A., Zschack P. and Dutta P., *Coll. and Surf. A*, **102**, 8790 (1995).
18. Lautz G. and Fischer Th.M., *J. Phys. Chem. B,* **101**, 8790 (1997).
19. Michaud F., Ventola L., Calvet M.T., Cuevas-Diarte M.A., Solans X. and Font-Bardia M., *Acta Cryst., **C**56*, 219 (2000).
20. Kolb D.M., in "*Structure of Electrified Interfaces*", Lipkowski J. and Ross P.N., (Eds), VCH, New York, 1993.
21. Kolb D.M., *Progress Surf. Sci.,* **51**, 109 (1996).
22. Wandlowski T., Ocko M., Magnussen O.M., Wu S. and Lipkowski J., *J. Electroanal. Chem.*, **409**, 155 (1996).
23. Wu S., Lipkowski J., Magnussen O.M., Ocko B.M. and Wandlowski Th., *J. Electroanal. Chem*., **44**, 667 (1998).
24. Majkrzak C.F., Ankner J.F., Berk N.F. and Gibbs D., In "*Magnetic Multilayers*", Bennett L.H., Watson R.E., (Eds), World Scientific Publishing Co, New Jersay, (1994) pp. 299–354.
25. Greenler R.G., *J. Chem. Phys.*, **44**, 310 (1966).
26. MacPhail R.A., Strauss H.L., Snyder R.G. and Elliger C.A., *J. Phys. Chem.,* **88**, 334 (1984).
27. MacPhail R.A., Snyder R.G. and Strauss H.L., *J. Chem. Phys*., **77**, 1118 (1982).
28. Snyder R.G., Strauss H.L. and Elliger C.A., *J. Phys. Chem*., **86**, 5145 (1982).
29. Allara D.L. and Swalen J.D., *J. Phys. Chem.,* **86**, 2700 (1982).
30. Umemura J., Kamata T., Kawai T. and Takenaka T., *J. Phys. Chem.*, **94**, 62 (1990).